

Superconductivity near 70 K in boron-carbon clathrates MB_2C_8 ($\text{M} = \text{Na}, \text{K}, \text{Rb}, \text{Cs}$) at ambient pressure

Bin Li,^{1,2,*} Yulan Cheng,³ Cong Zhu,³ Jie Cheng,^{1,2,†} and Shengli Liu¹

¹*School of Science, Nanjing University of Posts and Telecommunications, Nanjing 210023, China*

²*Jiangsu Provincial Engineering Research Center of Low Dimensional Physics and New Energy, Nanjing University of Posts and Telecommunications, Nanjing 210023, China*

³*College of Electronic and Optical Engineering, Nanjing University of Posts and Telecommunications, Nanjing 210023, China*
(Dated: May 24, 2024)

Inspired by the first boron-carbon (B-C) clathrate SrB_3C_3 and the ternary borohydride KB_2H_8 [Miao et al., Phys. Rev. B 104 L100504 (2021)], we have performed first-principles density functional theory calculations of the electronic and phonon band structures for B-C compounds MB_2C_8 ($\text{M} = \text{Na}, \text{K}, \text{Rb}, \text{Cs}$). Our calculations reveal that these materials are dynamically stable and can potentially exhibit superconductivity at ambient pressure. However, only the K, Rb, and Cs compounds exhibit thermodynamic stability below 50 GPa, while NaB_2C_8 remains thermodynamically unstable at all pressures considered. Based on the Allen and Dynes modified McMillan equation, we predict the superconducting transition temperature T_c of these compounds to be over 65 K at ambient pressure, with T_c decreasing under higher pressures. Remarkably, we find CsB_2C_8 possesses the highest predicted T_c of 68.76 K. Our findings demonstrate the possibility of high temperature superconductivity in cubic MB_2C_8 at ambient pressure, expanding the B-C clathrate superconductor family. These results provide valuable insights to guide the identification of new atmospheric pressure superconductors.

I. INTRODUCTION

Ashcroft *et al.* predicted that monatomic hydrogen would transform to the metallic state at high pressure with T_c reaching room temperature [1]. The experimental pressure required for the Wigner-Huntington transition to metallic hydrogen may be above 495 GPa [2, 3], which is currently too high to enable practical applications. In recent years, it has been theoretically proposed that metallic hydrogen can be prepared at lower pressure by "chemical precompression" [4], which can be achieved by adding other elements to the hydrogen, allowing the preparation of metallic hydrogen with much lower pressure. Many hydrogen-rich compounds containing main group elements have been considered as potential superconductors with high T_c in the past few years. A large number of binary and ternary hydrides have been theoretically predicted, and significant success has also been achieved experimentally [5–8]. For example, sulfur hydride (H_3S) was found to be superconducting at 203 K under 155 GPa [9, 10], and T_c of 250–260 K was observed in lanthanum hydride at 180–170 GPa [11, 12]. However, these binary hydride superconductors need to be formed under extremely high pressure to reach such high transition temperatures. Fortunately, some ternary hydrides, such as LaBH_8 [13], LaBH_9 [14], LaBeH_8 [15], CeBeH_8 and CeBH_8 [16] exhibit stronger "precompression" effects. These compounds are predicted to be potential superconductors and achieve high-temperature superconducting states at relatively low pressures, with some even dynamically stable down to 10 GPa.

However, the majority of the aforementioned hydrogen-rich compounds are formed under specific conditions, and maintaining their stability necessitates a certain pressure. They decompose under low pressures, making it challenging for these systems to exist stably at ambient pressure, which hinders the practical applications [17]. Recently, Zhu *et al.* achieved a significant breakthrough by successfully synthesizing a thermodynamically stable carbon-boron clathrate, SrB_3C_3 [18]. Their theoretical predictions suggested that this compound is a promising candidate for phonon-mediated superconductivity at ambient pressure. Subsequently, they embarked on a second round of predictions and synthesis, which confirmed the exceptional properties of SrB_3C_3 clathrate. Notably, this material exhibits a moderately high superconducting transition temperature (T_c) of approximately 22 K at 23 GPa, which is estimated to increase to a remarkable 31 K at ambient pressure [19]. In fact, theoretical calculations predict that all of the $Pm\bar{3}n$ XB_3C_3 alkaline earth analogues ($\text{X} = \text{Ca}, \text{Sr}, \text{Ba}$) exhibit remarkably high T_c in the range of 40–50 K at ambient pressure [20, 21]. Furthermore, the compound $\text{Rb}_{0.5}\text{Sr}_{0.5}(\text{BC})_3$ has been predicted to achieve an even higher T_c of approximately 75 K [22]. Compared to their hydride counterparts, boron-carbon superconductors exhibit a significant advantage: they require much lower pressure to achieve superconductivity. Remarkably, some boron-carbon superconductors can even reach a superconducting state at ambient pressure. This is attributed to the unique properties of boron and carbon, which are the lightest elements capable of forming strong covalent bonds. Materials based on these elements are known to be promising candidates for phonon-mediated superconductivity under ambient conditions [23]. Therefore, replacing hydrogen with

* Electronic addresses: libin@njupt.edu.cn

† Electronic addresses: chengj@njupt.edu.cn

other light elements is considered a feasible way to realize high- T_c superconductivity at ambient pressure.

In this work, we drew inspiration from a previous study [24], which predicted that the T_c of KB_2H_8 compound is 134-146 K at around 12 GPa. To obtain a stable and metallic compound, the authors intercalated a face-centered-cubic (FCC) lattice of potassium with BH_4 . On this basis, we envisioned replacing hydrogen with the element carbon to obtain new superconductors with lower pressures. We calculated the electronic band structure, phonon spectra and electron-phonon coupling and T_c in MB_2C_8 ($M = \text{Li, Na, K, Rb, Cs}$) by means of first-principles calculations. Our results indicate that the ambient pressure dynamical stability of MB_2C_8 simplifies experimental investigations and practical applications by eliminating the need for extreme pressure conditions.

II. COMPUTATIONAL DETAILS

The full structural optimization, including both the lattice parameters and atomic positions have been calculated within density functional theory as implemented in the QUANTUM ESPRESSO program [25]. Phonon and electron-phonon coupling matrix elements calculations have been carried out using density functional perturbation theory (DFPT) [26]. Pseudopotentials are selected from the Standard Solid State Pseudopotential (SSSP) library [27]. For self-consistent calculations, a $16 \times 16 \times 16$ k -point grid was used with an energy cutoff of 60 Ry for the wave functions and 480 Ry for the charge density. Dynamical matrices and electron-phonon coupling were calculated on an $8 \times 8 \times 8$ q -point mesh. A dense $24 \times 24 \times 24$ q grid was then used for evaluating an accurate electron-phonon interaction matrix. The effect of electron-phonon coupling on conventional superconductivity can be well represented by the Eliashberg function:

$$\alpha^2F(\omega) = \frac{1}{2\pi N(0)} \sum_{q\nu} \frac{\gamma_{q\nu}}{\omega_{q\nu}} \delta(\omega - \omega_{q\nu}), \quad (1)$$

Integrating the Eliashberg function over frequency, we can get the electron-phonon coupling λ :

$$\lambda(\omega) = 2 \int_0^\infty \frac{\alpha^2F(\omega)}{\omega} d\omega, \quad (2)$$

To estimate T_c , the Allen-Dynes modified McMillan equation [28] was used:

$$T_c = f_1 f_2 \frac{\omega_{log}}{1.2} \exp \left[-\frac{1.04(1 + \lambda)}{\lambda - \mu^*(1 + 0.62\lambda)} \right], \quad (3)$$

Coulomb pseudopotential μ^* is taken as 0.1 [29]. Electronic structure calculations were performed using the full-potential linearized augmented plane wave (FP-LAPW) method implemented in WIEN2k [30] with the Perdew-Burke-Ernzerhof (PBE) functional [31]. The muffin tin radius was chosen to be 2.3 a.u. for M, 1.47

a.u. for B and 1.46 a.u. for C, respectively. The $R \cdot K_{max} = 5.56$, with R is the smallest atomic sphere radius and K_{max} the largest K -vector. The crystal structure was visualized using VESTA [32], while Fermi surfaces were represented with Fermisurfer [33].

III. RESULTS AND DISCUSSION

Figure 1 illustrates the crystal structures of MB_2C_8 crystallizing in the cubic $Fm\bar{3}m$ space group (No. 225). The M, B and C atoms occupy the $4a$ (0.00, 0.00, 0.00), $8c$ (-0.25, 0.25, 0.25), and $32f$ ($-0.38 \pm u$, $0.38 \pm u$, $0.38 \pm u$) Wyckoff positions, respectively, where the variable u depends on pressure and the metal species M (see Table I). The boron and carbon atoms form a B_8C_{24} cage-like arrangement surrounding the metal atoms. We compute the formation enthalpies of the ternary carbides relative to decomposition into binary precursors, taking crystal structures of the binaries from the Materials Project database[34]: $Pm\bar{3}m$ (M, MB), $Immm$ (NaC), $Pm\bar{3}m$ (KC), $Pnma$ (RbC, CsC), $P6/mmm$ (RbC₈, CsC₈), $P63mc$ (BC), $P3m1$ (BC₅), and $P\bar{4}m2$ (BC₇) within 0-50 GPa. Pressure-dependent enthalpy differences are plotted in Fig. 2, showing that NaB_2C_8 is thermodynamically unstable up to 50 GPa while KB_2C_8 , RbB_2C_8 , and CsB_2C_8 decompose above 25, 25, and 40 GPa, respectively. Ambient and high-pressure lattice constants presented in Table I show unit cell volumes expand with increasing atomic number Z , while lattice parameters concurrently exhibit compression under pressure. Interatomic distances in Table II) demonstrate a corresponding reduction under applied pressure and enhancement as a function of increasing Z .

The thermodynamic stability of MB_2C_8 above 40 GPa motivate the examination of phononic properties. Phonon dispersions of $Fm\bar{3}m$ - MB_2C_8 ($M = \text{Li, Na, K, Rb, Cs}$) were calculated using the DFPT methodology at pressures of 0-50 GPa. The calculation results indicate stable phonon dispersion across the studied pressure regime with the sole exception of LiB_2C_8 (see Supplementary Figure S1 for Li data)[35]. The phonon dispersions and density of states at 40 GPa (Fig. 3) reveal dynamical stability under compression, evidenced by the absence of imaginary phonon frequencies along high-symmetry q path. The phonon spectra segregate into two regimes: (i) Low-frequency acoustic branches below 200 cm^{-1} stemming predominantly from alkali metal (M) atom oscillations, with heavier K, Rb, and Cs atoms inducing lower frequency modes. This manifests as the sharp low frequency peak in the density of states (DOS) plots. (ii) High-frequency optical branches between 500 - 1400 cm^{-1}

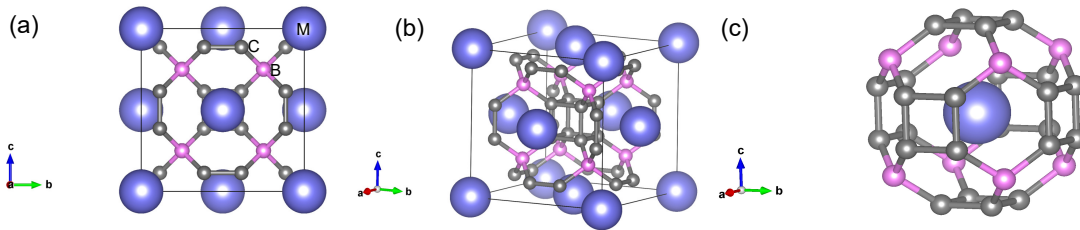


FIG. 1. (a) The top view and (b) side view of the crystal structure of MB_2C_8 , where M refers to an alkali metal. The blue, pink and gray spheres represent the M, boron, and carbon atoms, respectively. (c) The B_8C_{24} cage with M in the center.

TABLE I. Lattice constants and Wyckoff positions of MB_2C_8 (M = Na, K, Rb, Cs) at ambient pressure and 50 GPa.

M atoms	Pressure(GPa)	Lattice Parameters (Å)	Unit-cell volume (Å ³)	Wyckoff positions	Fractional coordinates
Na	0	a=b=c=6.9808	340.1854	B(8c)	-0.25000 0.25000 -0.25000
				C(32f)	-0.38621 0.38621 -0.38621
				Na(4a)	0.00000 0.00000 0.00000
	50	a=b=c=6.6109	288.9228	B(8c)	-0.25000 0.25000 -0.25000
				C(32f)	-0.38438 0.38438 -0.38438
				Na(4a)	0.00000 0.00000 0.00000
K	0	a=b=c=7.0237	346.4957	B(8c)	0.25000 -0.25000 0.25000
				C(32f)	0.38654 -0.38654 0.38654
				K(4a)	0.00000 0.00000 0.00000
	50	a=b=c=6.6508	294.1858	B(8c)	0.25000 -0.25000 0.25000
				C(32f)	-0.38465 0.38465 -0.38465
				K(4a)	0.00000 0.00000 0.00000
Rb	0	a=b=c=7.0640	352.4943	B(8c)	-0.25000 0.25000 0.25000
				C(32f)	-0.38685 0.38685 0.38688
				Rb(4a)	0.00000 0.00000 0.00000
	50	a=b=c=6.6894	299.3378	B(8c)	-0.25000 0.25000 0.25000
				C(32f)	-0.38494 0.38494 -0.38494
				Rb(4a)	0.00000 0.00000 0.00000
Cs	0	a=b=c=7.1266	361.9488	B(8c)	-0.25000 0.25000 0.25000
				C(32f)	-0.38736 0.38736 0.3873
				Cs(4a)	0.00000 0.00000 0.00000
	50	a=b=c=6.7467	307.0960	B(8c)	-0.25000 0.25000 0.25000
				C(32f)	-0.38536 0.38536 -0.38536
				Cs(4a)	0.00000 0.00000 0.00000

TABLE II. Atomic distances of B-C and C-C in MB_2C_8 at ambient pressure and 50 GPa.

	Pressure (GPa)	d_{B-C} (Å)	d_{C-C} (Å)
Na	0	1.6469	1.5887
	50	1.5387	1.5287
K	0	1.6611	1.5938
	50	1.5511	1.5343
Rb	0	1.6744	1.5986
	50	1.5635	1.5394
Cs	0	1.6955	1.6055
	50	1.5818	1.5469

associated with vibrations of the covalently bonded borocarbon cages. The alkali atom vibrations contribute primarily to acoustic modes and low-frequency density of states peaks, while the borocarbon cage vibrations dominate the higher frequency optical phonon branches. The

electron-phonon coupling enhancement from these high frequency B and C vibrations further influences emergent properties of select MB_2C_8 compounds under compression.

Analysis of the Γ -point optical branches reveals a declining maximum phonon frequency when progressing from lighter to heavier alkali metals in the MB_2C_8 compounds. The highest Γ -point optical frequency decreases from 1319.024 cm^{-1} in KB_2C_8 down to 1263.786 cm^{-1} for CsB_2C_8 . Meanwhile, a small gap emerges in the phonon spectra, separating low-frequency acoustic branches below 200 cm^{-1} from the higher optical branches. This gap widens as the alkali metal atomic number increases, spanning just 13.37 cm^{-1} in KB_2C_8 but reaching 59.76 cm^{-1} in CsB_2C_8 . As the atomic mass of the central metal increases, the lattice vibrations weaken, leading to a decrease in frequency and softening of low-frequency phonons. The widening of the gap is also attributable to the slight softening of low-frequency

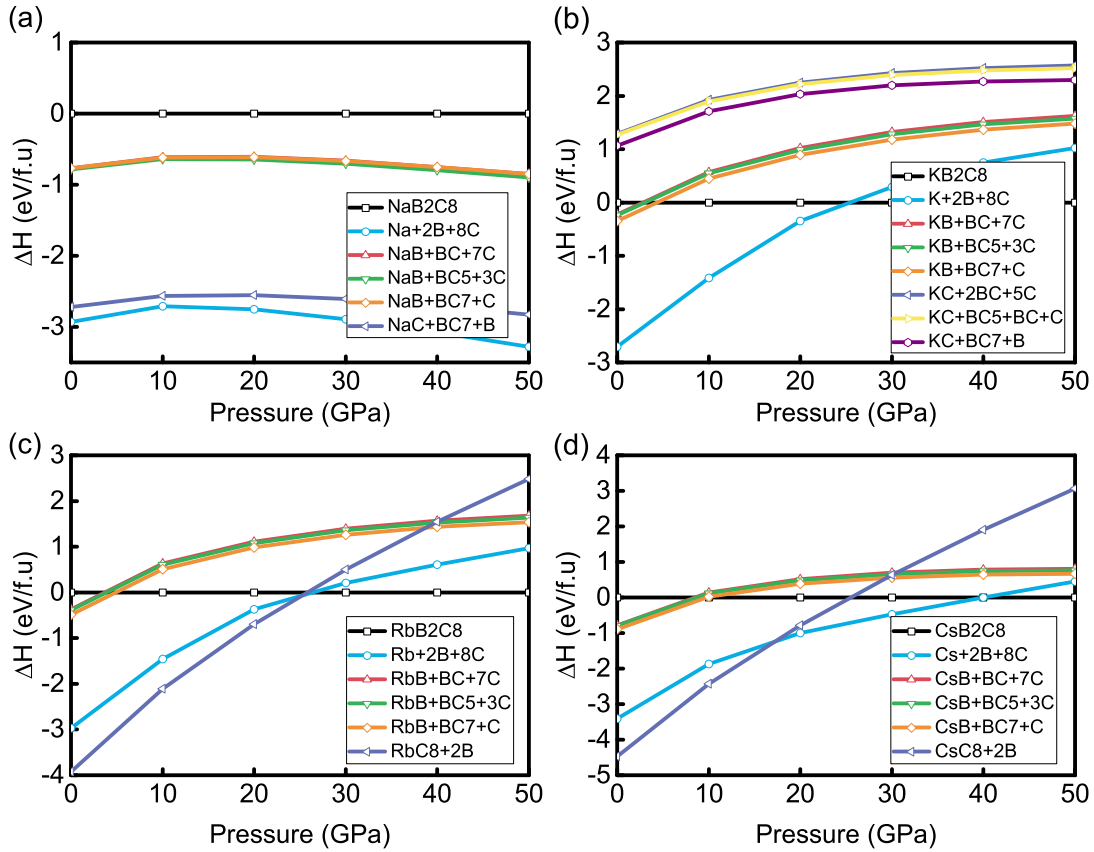


FIG. 2. Calculated enthalpy change (ΔH) as a function of pressure for MB_2C_8 compounds with $M = Na, K, Rb, Cs$. ΔH is referenced relative to the enthalpy of decomposition into standard elemental phases decompositions at the corresponding pressure. Other possible decomposition enthalpies were also considered. More negative ΔH indicates greater thermodynamic stability. Figures (a)-(d) show ΔH plots for NaB_2C_8 , KB_2C_8 , RbB_2C_8 , and CsB_2C_8 respectively

acoustic phonons. However, the effect of phonon softening on superconductivity varies under different pressure conditions. At ambient pressure, the superconducting transition temperature rises with increasing atomic mass, but it decreases at pressures around 50 GPa. This contrasting behavior may be related to the varying pressure dependence of the superconducting transition temperature for different central atoms.

The phonon density of states curves demonstrate that carbon atoms contribute more strongly than boron atoms. As shown in Figure 3, the alkali metal atoms do not significantly impact the electron-phonon coupling λ . In KB_2C_8 compound, vibrations of the B-C network account for approximately 87% of λ , while K atoms contribute only 13%. This suggests superconductivity arises predominantly from vibrations of the B-C sublattice. Phonon dispersion calculations reveal strong electron-phonon coupling between the X and W points in the Brillouin zone near 800 cm^{-1} , and the $W-L$ and $L-\Gamma$ directions also exhibit considerable coupling strength. The $L-\Gamma$ direction in the Brillouin zone around 600 cm^{-1} exhibits a relatively strong electron-phonon coupling strength, which is further enhanced in CsB_2C_8 .

The Eliashberg function, $\alpha^2F(\omega)$, contains three principal peaks that can be categorized into three frequency regions: $[400-600\text{ cm}^{-1}]$, $[600-1000\text{ cm}^{-1}]$, and $[1000-1400\text{ cm}^{-1}]$. Below 400 cm^{-1} , the electron-phonon coupling is weak, consistent with the minor contributions from alkali metal vibrations. In contrast, the predominant electron-phonon coupling intensity resides above the phonon frequency gap, arising primarily from vibrations of the B-C vibrations.

We calculated the electronic band structures and partial density of states projected onto individual atoms for MB_2C_8 ($M = K, Rb, Cs$) under pressure, shown in figure 4. Despite having different alkali metals M and external pressures, their band structures share similar characteristics, exhibiting metallic behavior with three bands crossing the Fermi level along the high-symmetry k path. In the region near the Fermi level, the DOS originates predominantly from the B and C atoms, with a greater contribution coming from the more electronegative C atoms [21]. Additionally, as the alkali metal changes from K to Rb to Cs, the indirect pseudo bandgap above the

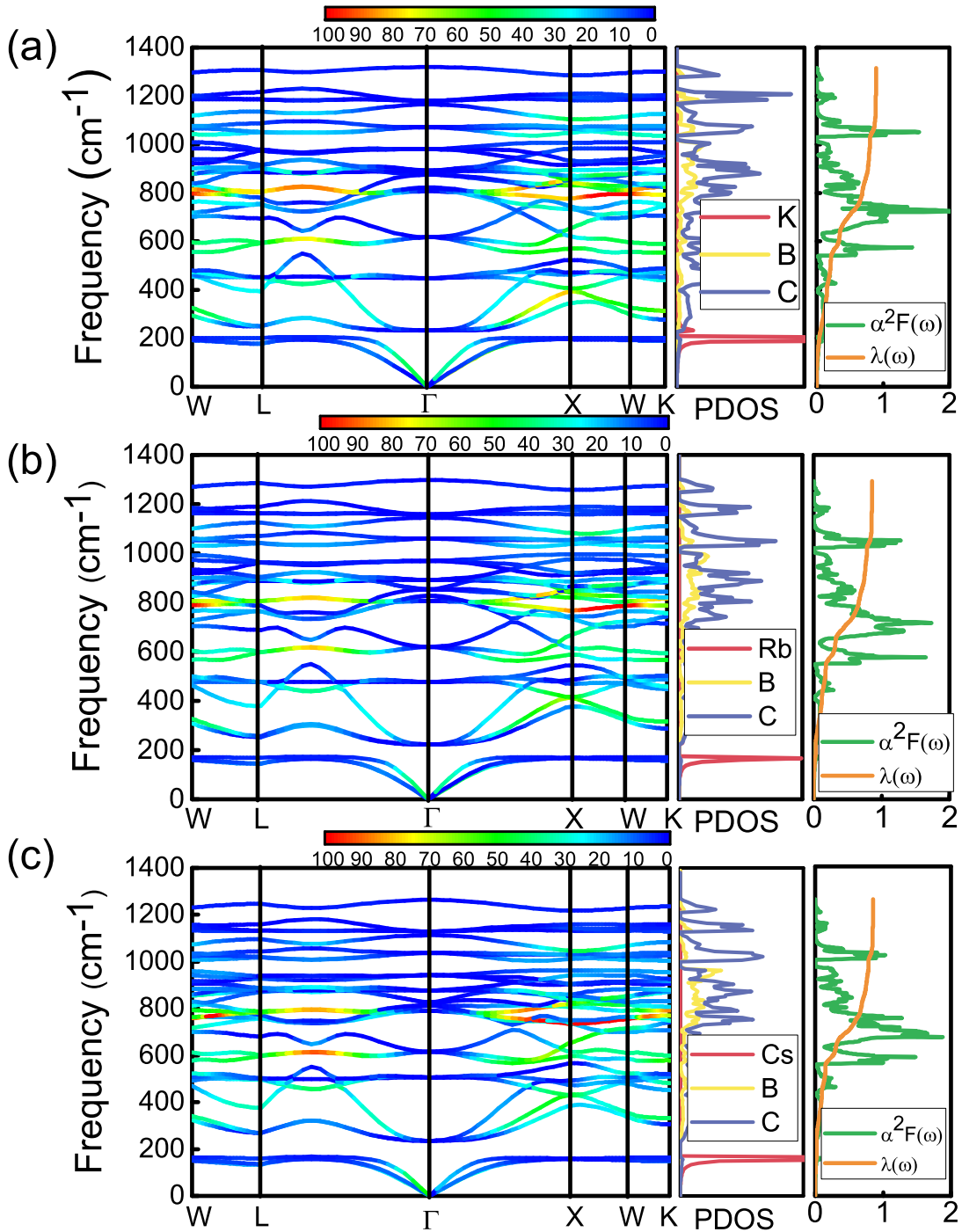


FIG. 3. (a-c) Phonon dispersion curves showing the phonon frequencies (ω_{qv}) with a color scale representing the phonon linewidths ($\lambda_{qv}\omega_{qv}$), the phonon density of states (PHDOS) projected onto individual atoms, the Eliashberg spectral function $\alpha^2F(\omega)$, and the electron-phonon coupling strength $\lambda(\omega)$ at 40 GPa for (a) KB_2C_8 , (b) RbB_2C_8 and (c) CsB_2C_8 . In the PHDOS plots, the projections onto the K, Rb, Cs (red), B (yellow), and C (blue) atoms are shown in different colors to distinguish the contributions of different atoms.

Fermi level increases progressively from 1.38 to 2.23 eV.

Figure 5 shows the band structure and corresponding Fermi surfaces (FSs) of CsB_2C_8 . The green, blue and yellow colored bands in Figure 5(a) correspond to the three

FSs shown in Figure 5(b). FS#1 has a dice-like morphology, with the minimum Fermi velocity at the vertex and maximum velocity at the center of each triangular face. FS#2 forms a concave cubic shape, with velocity maxima

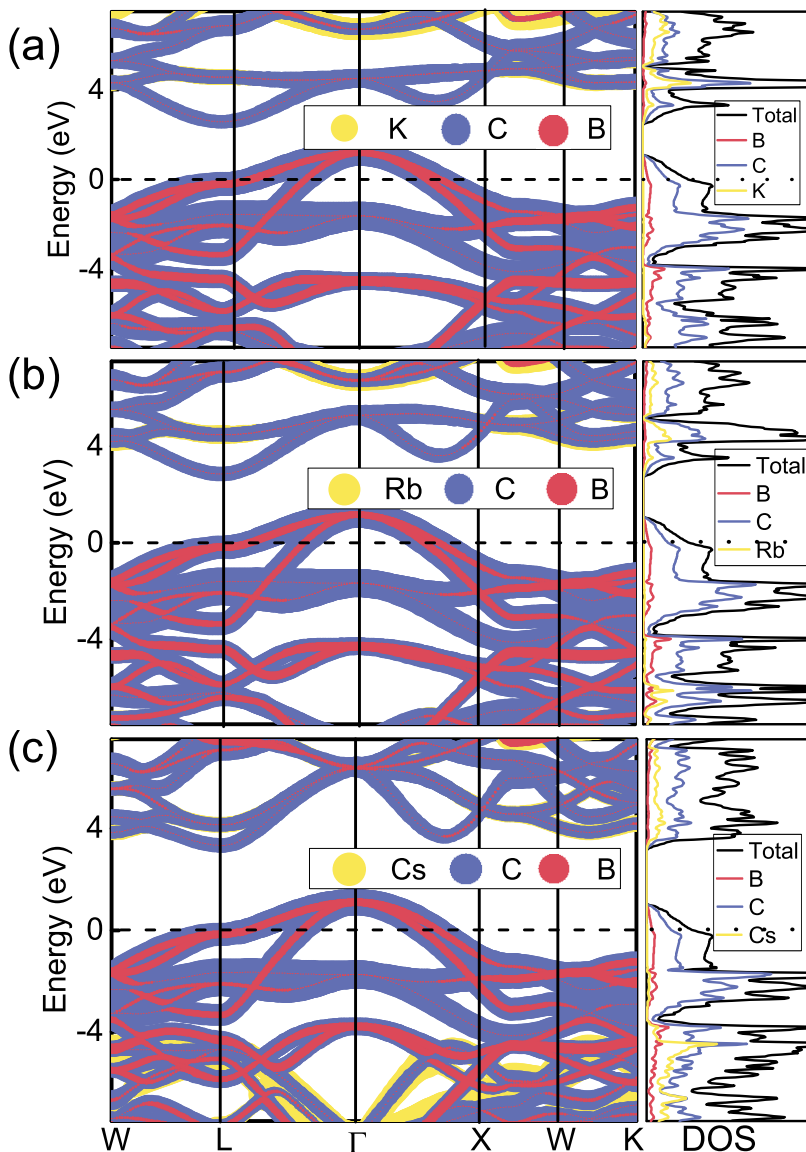


FIG. 4. Electronic band structures and partial density of states (DOS) projected on individual atomic species for MB_2C_8 ($M = K, Rb, Cs$) at 40 GPa pressure for KB_2C_8 , (b) RbB_2C_8 , and (c) CsB_2C_8 . In the DOS plots, the projections onto the M (K/Rb/Cs), B, and C atoms are shown in yellow, blue and red colors respectively. The Fermi energy is set to zero on the energy scale.

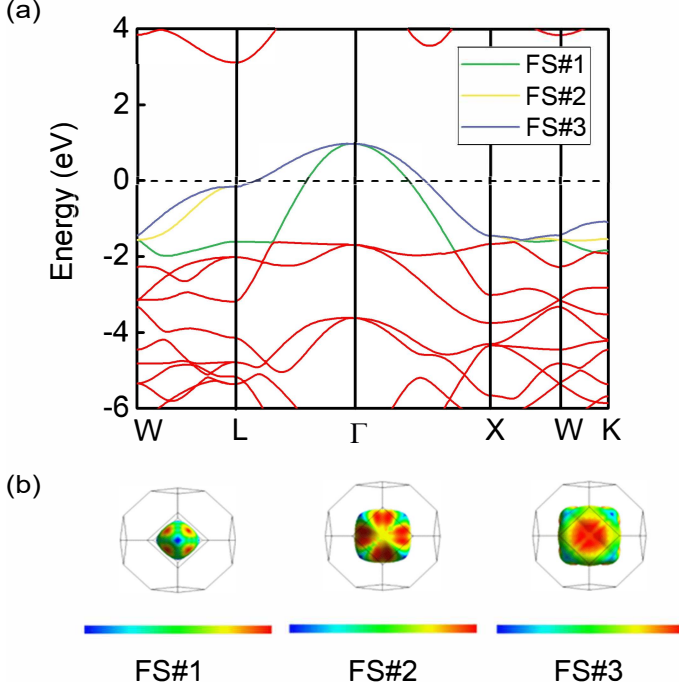
located at the inward-concave regions of each cube face. Lastly, FS#3 resembles a cubic morphology as well, but with both vertex and face-center regions concavely indented. For FS#3, the minimum velocities occur at the concave vertices while maximum velocities are found at the cube face centers.

The superconducting transition temperatures of MB_2C_8 at 0-50 GPa are listed in Table III, which exhibit a maximum predicted T_c of 68.76 K at 0 GPa in CsB_2C_8 . As external pressure rises from 0 to 50 GPa, T_c exhibits a declining trend. We also employed the original McMillan equation to estimate the superconducting

transition temperature, with the results presented in the supplementary material. The calculated superconducting transition temperature is slightly lower compared to the values reported in Table III. Figure 6(a) shows the electron-phonon coupling λ mirrors this pressure dependence, diminishing progressively across the same pressure range. However, as shown in Figure 6(b), the logarithmic average phonon frequency ω_{log} shows the opposite behavior, increasing with mounting pressure for the most cases. The one exception is NaB_2C_8 , for which ω_{log} declines after 20 GPa. At ambient pressure, substituting heavier alkali metals causes a slight enhancement in λ and T_c . However, contrasting different compounds at pressures

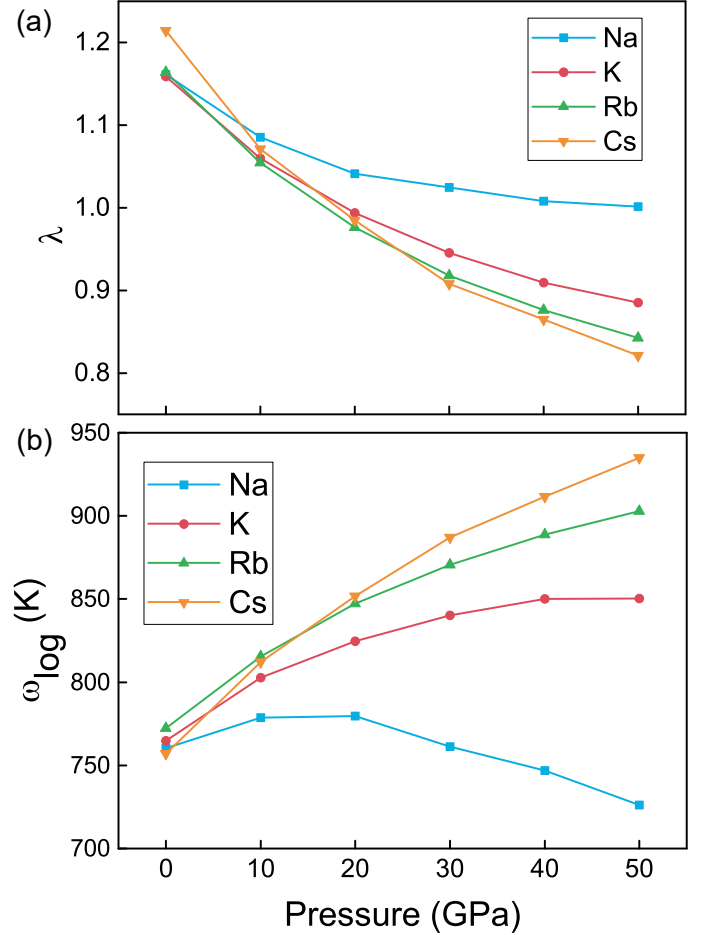
TABLE III. The calculated superconducting critical temperature T_c of MB_2C_8 ($M = Na, K, Rb, Cs$) at various pressures.

	T_c (K)					
	0 (GPa)	10 (GPa)	20 (GPa)	30 (GPa)	40 (GPa)	50 (GPa)
Na	65.30	61.13	57.69	55.00	52.66	50.68
K	65.55	60.92	56.90	53.52	50.69	48.36
Rb	66.56	61.47	56.86	52.78	49.61	46.85
Cs	68.76	62.59	57.91	52.79	49.67	46.16


 FIG. 5. (a) Electronic band structures of CsB_2C_8 at 40 GPa. (b) The three Fermi surfaces (FS#1, FS#2, FS#3) derived from bands crossing the Fermi level in (a). The FS contours are colored according to the Fermi velocities.

exceeding 20 GPa reveals that substituting heavier alkali metals causes a slight reduction in λ and T_c , while ω_{log} increases progressively down the alkali metal series from Na to Cs. Given the consistent correlation observed between the pressure and alkali metal dependence of both T_c and λ , it can be inferred that the electron-phonon coupling strength plays the predominant role in influencing the superconducting transition temperature.

In summary, we employed first-principles methods to investigate the fundamental properties of the alkali metal-boron-carbon compound MB_2C_8 ($M = Li, Na, K, Rb, Cs$) across a pressure range of 0-50 GPa. Our findings indicate that all compounds, except for LiB_2C_8 , reside in a metastable state under ambient conditions. Notably, MB_2C_8 ($M = Na, K, Rb, Cs$) exhibits dynamic stability within this pressure range, while NaB_2C_8 is thermodynamically unstable. KB_2C_8 and RbB_2C_8 become thermodynamically stable at pressures exceeding


 FIG. 6. (a) Calculated electron-phonon coupling constant λ , and (b) logarithmic average of phonon frequency ω_{log} for MB_2C_8 ($M = Na, K, Rb, Cs$) as a function of pressure.

25 GPa, while CsB_2C_8 forms with a positive enthalpy at 40 GPa, suggesting their potential synthesis at high pressures followed by quenching to ambient conditions. Electron-phonon calculations which mainly from vibrations of borocarbon cage, indicate that MB_2C_8 compounds could exhibit superconductivity with a maximum critical temperature of 68.76 K at ambient pressure. Our prediction of these novel MB_2C_8 compounds opens up further possibilities for the application of ternary B-C clathrates.

ACKNOWLEDGMENTS

This work is supported by the National Natural Science Foundation of China (Grants No. 12175107)

and Nanjing University of Posts and Telecommunications Foundation (NUPTSF) (Grant No. NY219087, NY220038). Some of the calculations were performed on the supercomputer in the Big Data Computing Center (BDCC) of Southeast University.

-
- [1] N. W. Ashcroft, *Physical Review Letters* **21**, 1748 (1968).
 [2] R. P. Dias and I. F. Silvera, *Science* **358**, eaao5843 (2017).
 [3] X.-D. Liu, P. Dalladay-Simpson, R. T. Howie, B. Li, and E. Gregoryanz, *Science* **357**, aan2286 (2017).
 [4] K. P. Hilleke and E. Zurek, *Journal of Applied Physics* **131**, 070901 (2022).
 [5] H. Wang, J. S. Tse, K. Tanaka, T. Iitaka, and Y. Ma, *Proceedings of the National Academy of Sciences of the United States of America* **109**, 6463 (2012).
 [6] K. Abe, *Physical Review B* **103**, 134118 (2021).
 [7] D. Duan, Y. Liu, F. Tian, D. Li, X. Huang, Z. Zhao, H. Yu, B. Liu, W. Tian, and T. Cui, *Scientific Reports* **4**, 6968 (2014).
 [8] H. Xie, D. Duan, Z. Shao, H. Song, Y. Wang, X. Xiao, D. Li, F. Tian, B. Liu, and T. Cui, *Journal of Physics-Condensed Matter* **31**, 245404 (2019).
 [9] A. P. Drozdov, M. I. Erements, I. A. Troyan, V. Ksenofontov, and S. I. Shylin, *Nature* **525**, 73 (2015).
 [10] Y. Yao and J. S. Tse, *Chemistry-a European Journal* **24**, 1769 (2018).
 [11] A. P. Drozdov, P. P. Kong, V. S. Minkov, S. P. Besedin, M. A. Kuzovnikov, S. Mozaffari, L. Balicas, F. F. Balakirev, D. E. Graf, V. B. Prakapenka, E. Greenberg, D. A. Knyazev, M. Tkacz, and M. I. Erements, *Nature* **569**, 528 (2019).
 [12] M. Somayazulu, M. Ahart, A. K. Mishra, Z. M. Geballe, M. Baldini, Y. Meng, V. V. Struzhkin, and R. J. Hemley, *Physical Review Letters* **122**, 027001 (2019).
 [13] S. Di Cataldo, C. Heil, W. von der Linden, and L. Boeri, *Physical Review B* **104**, L020511 (2021).
 [14] X. Liang, A. Bergara, X. Wei, X. Song, L. Wang, R. Sun, H. Liu, R. J. Hemley, L. Wang, G. Gao, and Y. Tian, *Physical Review B* **104**, 134501 (2021).
 [15] Z. Zhang, T. Cui, M. J. Hutcheon, A. M. Shipley, H. Song, M. Du, V. Z. Kresin, D. Duan, C. J. Pickard, and Y. Yao, *Physical Review Letters* **128**, 047001 (2022).
 [16] Y. Hou, B. Li, Y. Bai, X. Hao, Y. Yang, F. Chi, S. Liu, J. Cheng, and Z. Shi, *Journal of Physics-Condensed Matter* **34**, 505403 (2022).
 [17] H. B. Ding, Y.-J. Feng, M.-J. Jiang, H.-L. Tian, G.-H. Zhong, C.-L. Yang, X.-J. Chen, and H.-Q. Lin, *Physical Review B* **106**, 104508 (2022).
 [18] L. Zhu, G. M. Borstad, H. Liu, P. A. Gunka, M. Guerette, J.-A. Dolyniuk, Y. Meng, E. N. Greenberg, V. B. Prakapenka, B. L. Chaloux, A. Epshteyn, R. E. Cohen, and T. A. Strobel, *Science Advances* **6**, aay8361 (2020).
 [19] L. Zhu, H. Liu, M. Somayazulu, Y. Meng, P. A. Gunka, T. B. Shiell, C. Kenney-Benson, S. Chariton, V. B. Prakapenka, H. Yoon, J. A. Horn, J. Paglione, R. Hoffmann, R. E. Cohen, and T. A. Strobel, *Physical Review Research* **5**, 013012 (2023).
 [20] S. Di Cataldo, S. Qulaghasi, G. B. Bachelet, and L. Boeri, *Physical Review B* **105**, 064516 (2022).
 [21] J.-N. Wang, X.-W. Yan, and M. Gao, *Physical Review B* **103**, 144515 (2021).
 [22] P. Zhang, X. Li, X. Yang, H. Wang, Y. Yao, and H. Liu, *Physical Review B* **105**, 094503 (2022).
 [23] N. Geng, K. P. Hilleke, L. Zhu, X. Wang, T. A. Strobel, and E. Zurek, *Journal of the American Chemical Society* **145**, 1696 (2023).
 [24] M. Gao, X.-W. Yan, Z.-Y. Lu, and T. Xiang, *Physical Review B* **104**, L100504 (2021).
 [25] P. Giannozzi, S. Baroni, N. Bonini, M. Calandra, R. Car, C. Cavazzoni, D. Ceresoli, G. L. Chiarotti, M. Cococcioni, I. Dabo, A. Dal Corso, S. de Gironcoli, S. Fabris, G. Fratesi, R. Gebauer, U. Gerstmann, C. Gougoussi, A. Kokalj, M. Lazzeri, L. Martin-Samos, N. Marzari, F. Mauri, R. Mazzarello, S. Paolini, A. Pasquarello, L. Paulatto, C. Sbraccia, S. Scandolo, G. Sclauzero, A. P. Seitsonen, A. Smogunov, P. Umari, and R. M. Wentzcovitch, *Journal of Physics-Condensed Matter* **21**, 395502 (2009).
 [26] S. Baroni, S. de Gironcoli, A. Dal Corso, and P. Giannozzi, *Reviews of Modern Physics* **73**, 515 (2001).
 [27] G. Prandini, A. Marrazzo, I. E. Castelli, N. Mounet, and N. Marzari, *Npj Computational Materials* **4**, 72 (2018).
 [28] P. B. Allen and R. C. Dynes, *Physical Review B* **12**, 905 (1975).
 [29] Y. Yao, J. S. Tse, K. Tanaka, F. Marsiglio, and Y. Ma, *Physical Review B* **79**, 054524 (2009).
 [30] P. Blaha, K. Schwarz, P. Sorantin, and S. B. Trickey, *Computer Physics Communications* **59**, 399 (1990).
 [31] J. P. Perdew, K. Burke, and M. Ernzerhof, *Physical Review Letters* **77**, 3865 (1996).
 [32] K. Momma and F. Izumi, *Journal of Applied Crystallography* **44**, 1272 (2011).
 [33] M. Kawamura, *Computer Physics Communications* **239**, 197 (2019).
 [34] A. Jain, S. P. Ong, G. Hautier, W. Chen, W. D. Richards, S. Dacek, S. Cholia, D. Gunter, D. Skinner, G. Ceder, and K. A. Persson, *APL Materials* **1**, 011002 (2013).
 [35] See supplemental material at <http://link.aps.org/supplemental/xxxx> for additional phonon spectra.